JGR Atmospheres

RESEARCH ARTICLE
10.1029/2023JD040667

The Effects of Summer Snowfall on Arctic Sea Ice Radiative Forcing

H. R. Chapman-Dutton[1] and **M. A. Webster**[2]

[1]Geophysical Institute, University of Alaska Fairbanks, Fairbanks, AK, USA, [2]Applied Physics Laboratory, Polar Science Center, University of Washington, Seattle, WA, USA

Key Points:

- Ephemeral summer snowfall increased albedo by 0.08 and decreased TOA radiative forcing by 0.086 ± 0.020 W m^{-2} across the Arctic Ocean in 2003–2017
- The average snow accumulation event led to a ~2 cm increase in snow depth and lasted 3.4 days
- Optically thick (>3 cm) snow accumulation events occurred in 16.5% of all events and lasted 6.3 days

Supporting Information:

Supporting Information may be found in the online version of this article.

Correspondence to:

H. R. Chapman-Dutton,
hchapmandutton@gmail.com

Citation:

Chapman-Dutton, H. R., & Webster, M. A. (2024). The effects of summer snowfall on Arctic sea ice radiative forcing. *Journal of Geophysical Research: Atmospheres*, *129*, e2023JD040667. https://doi.org/10.1029/2023JD040667

Received 21 DEC 2023
Accepted 28 JUN 2024

Author Contribution:

Conceptualization: M. A. Webster
Funding acquisition: M. A. Webster
Methodology: M. A. Webster
Supervision: M. A. Webster
Writing – review & editing: M. A. Webster

Abstract Snow is the most reflective natural surface on Earth. Since fresh snow on bare sea ice increases the surface albedo, the impact of summer snow accumulation can have a negative radiative forcing effect, which would inhibit sea ice surface melt and potentially slow sea-ice loss. However, it is not well known how often, where, and when summer snowfall events occur on Arctic sea ice. In this study, we used in situ and model snow depth data paired with surface albedo and atmospheric conditions from satellite retrievals to characterize summer snow accumulation on Arctic sea ice from 2003 to 2017. We found that, across the Arctic, ~2 snow accumulation events occurred on initially snow-free conditions each year. The average snow depth and albedo increases were ~2 cm and 0.08, respectively. 16.5% of the snow accumulation events were optically thick (>3 cm deep) and lasted 2.9 days longer than the average snow accumulation event (3.4 days). Based on a simple, multiple scattering radiative transfer model, we estimated a -0.086 ± 0.020 W m^{-2} change in the annual average top-of-the-atmosphere radiative forcing for summer snowfall events in 2003–2017. The following work provides new information on the frequency, distribution, and duration of observed snow accumulation events over Arctic sea ice in summer. Such results may be particularly useful in understanding the impacts of ephemeral summer weather on surface albedo and their propagating effects on the radiative forcing over Arctic sea ice, as well as assessing climate model simulations of summer atmosphere-ice processes.

Plain Language Summary As sea ice declines in the Arctic, it is necessary to understand the role that sea ice plays in the Arctic climate. During summer, ice is particularly important because it acts as a barrier between the atmosphere and ocean, and shields the ocean from sunlight. Sea ice is a surface on which snowfall can accumulate. Since snow is the most reflective natural surface on earth, its presence during the sunny season can reflect significant amounts of sunlight away from the earth's surface and reduce warming. In this work, we studied the impact of summer snowfall on sea ice by combining data from buoys, satellites, and models to determine how much sunlight is reflected by short-lived summer snow accumulation on Arctic sea ice. We learned that the average snow event raises the reflectivity of the surface by 0.08 with ~2 cm of snow depth change. Events with more than 3 cm of accumulation lasted ~3 days longer than average (~3 days). Overall, summer snow accumulation reduces the amount of energy absorbed by the Arctic region by 0.086 W m^{-2} each year. These results help to improve our understanding of the Arctic climate and may also be useful for evaluating climate models.

1. Introduction

Fresh snow is the most reflective natural material on earth (Warren, 2019). In the Arctic, bare sea ice has a high albedo (a) of 0.65–0.70, but the albedo of fresh snow can be between 0.80 and 0.90 (Light et al., 2022; Perovich, Nghiem, et al., 2007; Perovich & Polashenski, 2012). A typical ice-dominated region of the ocean in the summer months may include many combinations of bare sea ice, snow, and melt ponds. During the peak of summer, undeformed seasonal ice can have over 50% of its surface area covered by melt ponds (Fetterer & Untersteiner, 1998; Polashenski et al., 2012; Scharien & Yackel, 2005; Webster et al., 2015). As multiyear ice cover decreases and smoother seasonal ice becomes dominant across the Arctic, we could see a 38% increase in solar heat input to the ice layer and subsequently, to the upper ocean, if pond coverage were to correspondingly increase (Perovich & Polashenski, 2012). This extra heat has implications for sea ice mass balance and sea surface temperatures (Stroeve et al., 2014) as well as for ocean circulation and primary productivity in the Arctic Ocean (Post et al., 2013). However, if fresh snow accumulates on top of sea ice in summer, the solar absorption within sea ice and the ocean could be strongly mitigated.

Table 1
Key Variables and Sources

Data product	Key variables	Reference
Sea ice mass balance buoys	Snow depth (m)	http://imb-crrel-dartmouth.org (Perovich et al., 2023)
	Air temperature (°C)	
	Air pressure (hPa)	
Ice parcel database (Horvath et al., 2023)	SnowModel-LG (ERA5) Snow Depth (m)	Liston et al. (2020)
	NSIDC Sea Ice Concentration (%)	Fetterer et al. (2017)
	ERA5 Surface Air Temperature (°C)	Hersbach et al. (2023)
	ERA5 850 hPa Air Temperature (°C)	
	CERES Surface Albedo	Wielicki et al. (1996)
Melt pond distribution on sea ice	Melt Pond Fraction (%)	Rösel et al. (2015)

Note. All values have been calculated to daily averages.

Relatively little is known about summer snowfall on Arctic sea ice. Most research on this topic relates to the winter months, but a few studies have documented individual summer snowfall events and the effects that they can have on the progression of ice melt (Light et al., 2015; Lim et al., 2022; Perovich et al., 2002, 2017). The 19 June 1998 snowfall during the Surface Heat Budget of the Arctic Ocean (SHEBA) expedition is a well-documented example of such an event during which four cm of fresh snow caused an increase in albedo from 0.20 to 0.80 over areas of bare sea ice and refrozen ponds before returning to pre-snow values two days later (Perovich et al., 2002). In a different event described in Perovich et al. (2017), an early June snowfall delayed the ice surface melt onset by several weeks. While the albedo impact of this snowfall was relatively small and short-lived (increasing from 0.68 to 0.77), the latent heat associated with melting the new snow caused the snow layer to act as a negative heat flux and therefore protect the underlying ice from surface melt.

A study by Lim et al. (2022) used satellite retrievals, reanalysis products, and a sea ice model to investigate summer snowstorms in the North Atlantic and Eurasian-Pacific regions of the Arctic between 1980 and 2019. The results showed that the 95–96 documented storms increased the surface albedo by 0.01–0.02 over the Central Arctic region and reduced the shortwave absorption by ∼2 W m^{-2}. Lim et al. (2022) found that the snowstorms were also associated with about a week of below-freezing surface air temperatures, which allowed the new snow to persist. Using a sea ice model, they found that cold temperatures were the main driver behind a positive sea ice extent anomaly of 1.2×10^5 km^2 associated with snowstorms. Even so, the model simulations suggested that snowfall explained about 25% of the ice extent anomaly, with the remaining effect relating to cold air temperatures.

As a result of sparse in situ observations, several knowledge gaps remain about the nature of summer snow accumulation on Arctic sea ice: how frequently does summer snow accumulation occur, how much snow accumulates, how long does the snow cover last, and what are the impacts of summer snow accumulation events on the surface energy balance. This study aims to address these knowledge gaps by using in situ, model, and remotely sensed data to characterize summer snow accumulation events between 2003 and 2017. We leverage a newly developed Lagrangian ice parcel database (Horvath et al., 2023) to quantify the frequency, amount, duration, and effect of summer snow accumulation on Arctic sea ice. We approached the study of summer snow on Arctic sea ice with the objective of answering the question: how do summer snowfall events impact the surface albedo of Arctic sea ice? Within this broader question, we also investigated the impact of snow layer thickness, regional differences in summer snow cover, and how the presence of melt ponds and changing ice concentrations could affect surface albedo.

2. Data

This analysis focuses on sea ice, snow, and atmospheric data from 2003 through 2017 to investigate the impacts of snow accumulation on Arctic summer sea ice. To do this, a variety of complementary data sets are used, ranging from direct surface measurements from buoys to satellite retrievals and model output. Each data type used in the analysis is described below and listed in Table 1. The analysis is presented at two spatial scales: the local scale,

using buoy data (Sections 2.1, 3.1, and 4.1) and the pan-Arctic scale, using the ice parcel database (Sections 2.2, 3.2, and 4.2). In this way, the analysis starts at the local scale and then expands up to the pan-Arctic scale.

2.1. Local Scale Data: Ice Mass Balance Buoys

We began our study of summer snow accumulation at the local scale with in situ observations of snow depth, air temperature, and surface air pressure. The Cold Regions Research and Engineering Laboratory (CRREL)-Dartmouth Ice Mass Balance Buoys (IMBs) (Perovich et al., 2023) provide multiple time-series' beginning in 1997 and extending through 2018. While the specific instrumentation can vary, the basic buoy sensors include an air temperature probe, thermistor string, barometer for sea level pressure, and two acoustic sounders facing upwards and downwards to measure snow depth and ice draft. The sounders can measure snow depth and ice draft changes down to 5 mm, but have an inherent uncertainty of about 1 cm (Perovich et al., 2023). Buoys are most often deployed in the Central Arctic and the Beaufort Sea and are left to drift with the sea ice. Data are recorded every one or 4 hours; the snow depths have been averaged to daily values for the purposes of this study.

2.2. Pan-Arctic Scale Data: Ice Parcel Database

We expanded the analysis to the pan-Arctic scale to understand the larger scale effects of snow accumulation on sea ice using remote sensing, reanalysis, and model data. The Ice Parcel Database (Horvath et al., 2023) takes a Lagrangian approach to tracking sea ice as it drifts throughout the Arctic. Each 25-km by 25-km parcel represents a grid cell with an ice concentration of at least 15%. The parcels are tracked from October through to the end of September each year from 2002 to 2020. The database was created by combining multiple satellite, model, and reanalysis data products and includes a wide range of information about each ice parcel, including radiative forcing and energy balance terms. All incorporated data in the Lagrangian ice parcel database have been re-gridded to a 25-km resolution. The primary variables used in this analysis are the Clouds and Earth's Radiant Energy System (CERES) calculated surface albedo product (Wielicki et al., 1996), NOAA/NSIDC Climate Data Record sea ice concentration (Fetterer et al., 2017), surface and 850 hPA air temperature from the fifth generation European Center for Medium-Range Weather Forecasts (ERA5) reanalysis product (Hersbach et al., 2023), and snow depth simulated by SnowModel-LG (Liston et al., 2020). We evaluated the summers of 2003–2017 for consistent temporal coverage of the IMB data used in this study.

2.3. SnowModel-LG

Within the ice parcel database, we use snow depths generated by SnowModel-LG (Liston et al., 2020) for the pan-Arctic scale analysis. These values are calculated using ERA5 liquid water equivalent precipitation mass flux along with air temperature, relative humidity, and wind speed and direction (Liston et al., 2020). This model accounts for snow accumulation and melt, as well as other processes such as blowing snow redistribution, rainfall, superimposed ice, density evolution, snow grain metamorphism, and sublimation. The predecessor to ERA5, Era-Interim has been shown to underestimate Arctic snowfall (Edel et al., 2020). In the fifth generation, ERA5 cloud microphysics schemes have been improved, yielding higher snowfall amounts in the Arctic Ocean domain relative to ERA-Interim (Boisvert et al., 2023; Cabaj et al., 2020; Wang et al., 2019); however, relative to observations, a low bias still exists, and the ERA5 precipitation is scaled by a factor >1 in SnowModel-LG to align with snow depth observations more closely (see Section 2.5 in Liston et al., 2020 for more details).

To better understand the propagating biases of ERA5 reanalysis on the SnowModel-LG performance in summer, we examined time-series from 54 ice mass balance buoys for 1993–2017 that had partial or full coverage of the June–August period. We compare all summer snow accumulation events between the buoys and model, regardless of the surface being initially snow-free. The model snow accumulations were thinner by 4 cm on average (11 vs. 7 cm, respectively). However, the duration of summer snow accumulation was similar between observations and the model output (14 ± 8 and 11 ± 4 days, respectively). Given the large albedo effect from snow-free conditions to even a thin layer of snow (Brandt et al., 2005), our comparisons suggest that there is sufficient snow accumulation and snow cover duration in the model results to characterize summer snowfall events to investigate the radiative effects over Arctic sea ice.

3. Methods

Using daily average snow depths from the IMB buoys and SnowModel-LG output, we defined summer snow accumulation events across the Arctic based on the following criteria: (a) occurrence in May–August, (b) the surface was initially snow-free (one cm or less snow depth), (c) there was at least one cm of new snow accumulation, and (d) a subsequent melt period occurred that reduced the snow depth to one cm or less. Events that showed an accumulation of three cm or more were classified as being optically thick based on the results and data from Perovich (2007).

3.1. Local Scale

Case studies from the IMB buoys serve as an in situ baseline for this study. Out of the 64 buoys evaluated, 16 summer snow accumulation events were identified. Seven of the buoys recorded the same storm as another buoy. Thus, there is a total of 12 distinct weather events resulting in snow accumulation over nearly snow-free conditions at the buoys. Specifics of each case study can be found Table S1 in Supporting Information S1. For each selection, the total snow accumulation was determined, as well as the number of days that passed before the snow melted completely or returned to the initial depth of 1 cm or less. In some cases when a snow accumulation event occurred near the end of the summer season, it formed the first layer of the winter snowpack and remained through the end of the year. These cases were not included in the calculation of the average duration of snow accumulation events.

We combined the IMB and ice parcel data for each case study to determine the albedo response to the new snow accumulation, changes in total precipitation and atmospheric conditions (pressure, temperature, wind speeds), and to compare the in situ snow accumulation amount and duration with that from the SnowModel-LG output (within the ice parcel database). Coincident ice parcels to the buoys were found, and, while the buoys do not line up precisely with the parcel drift track at times, they remain within 100 km of each other (Horvath et al., 2023). The largest separation between the buoys and ice parcels occurs in the Fram Strait region and is attributed to an underestimation of ice drift in this region (Sumata et al., 2014).

3.2. Pan-Arctic Scale

We expanded the analysis to the pan-Arctic scale using the ice parcel database to quantify how often summer snow accumulation occurs, how long the new snow cover lasts, what areal coverage the accumulation events have, and what impacts the new snow has on surface albedo. For all events, we analyzed the atmospheric characteristics, ice properties, and the duration of the event. We divided the parcels into regions following the region mask in Meier et al. (2007) to determine the geographic differences of snow accumulation events across the Arctic. Southerly regions such as the Bering and Okhotsk seas, Baffin Bay, Hudson Bay, and the Gulf of St. Lawrence were not included as they are unlikely to maintain sea ice in the summer months.

3.3. Radiative Forcing Impacts

We used a simple two-layer reflectance model (Thomas & Stamnes, 1999, Section 6.11) to compute the change in the top-of-the-atmosphere (TOA) radiative forcing resulting from the addition of a fresh snow layer on top of melting, bare sea ice. In this way, we determined how much the TOA albedo changed during summer snowfall events and the resulting amount of additional radiation reflected back into space.

The methodology presented here largely follows those presented in Webster and Warren (2022); specifically, we use the same two-layer multiple reflection model (Thomas & Stamnes, 1999, Section 6.11) and the following values and assumptions: (a) the Arctic climatological cloud cover is 80% in space and time (Environmental Working Group, 2000); (b) the monthly climatological TOA solar irradiance follows those in Hartmann (2016) and is area-weighted over 70–90°N latitude; (c) the snow transmittance under clear and cloudy skies is estimated from Perovich (2007); (d) albedo values for different surface types (fresh thin snow; bare melting sea ice; melt ponds) under clear and cloudy sky conditions are based on observed values from Perovich (2007), and Perovich and Polashenski (2012), and Light et al. (2022); and (e) the area of the Arctic Ocean is defined by the Meier et al. (2007) region mask. Values for these conditions and variables, as well as other details on the methodology, can be found in Webster and Warren (2022) and albedo values are additionally listed in Table 2. We assume an

Table 2
Variables and Values Used in Calculating the Radiative Forcing Impact of Summer Snow Accumulation Events

		Clear sky	Cloudy sky
a_{snow}	Fresh Snow Albedo	0.80	0.86
t_{snow}	Fresh Snow Transmittance	0.027	0.038
a_{ice}	Bare Ice Albedo	0.58	0.63
a_{atm}	Atmospheric Albedo	0.14	0.51
t_{atm}	Atmospheric Transmittance	0.76	0.42

uncertainty of 0.02 for all albedo and transmittance values. Further explanation of the atmospheric albedo and transmittance can be found Table S3 in Supporting Information S1.

To determine the TOA albedo change, broadband albedo values for two surface conditions (thin, fresh snow vs. bare, melting ice) are first considered in clear versus cloudy conditions. Equation 1a is the two-layer multiple reflection model for the system (combined) albedo (Thomas & Stamnes, 1999) of fresh, thin snow (with an albedo, a_{snow}, and transmittance, t_{snow}) on top of bare ice (a_{ice}). This surface system albedo (a_{surf}) is calculated using the corresponding albedo and transmittance values of snow and ice (Table 2) for both clear and cloudy conditions separately. We then repeat the calculation using the surface system albedo (a_{surf}) as the lower layer and the atmospheric albedo (a_{atm}) and transmittance (t_{atm}) as the upper layer (Equation 1b) to determine the TOA system albedo (a_{sys}).

$$a_{surf} = a_{snow} + \frac{a_{ice}\ t_{snow}^2}{1 - a_{ice}\ a_{snow}} \tag{1a}$$

$$a_{sys} = a_{atm} + \frac{a_{surf}\ t_{atm}^2}{1 - a_{surf}\ a_{atm}} \tag{1b}$$

Using the TOA system albedo of fresh snow on bare ice ($a_{sys_{clear}}$; $a_{sys_{cloudy}}$), we calculated the change in albedo when going from bare ice to full snow cover under both sky conditions.

$$\Delta a_{sys_{clear}} = a_{sys_{clear}} - a_{ice_{clear}} \tag{2a}$$

$$\Delta a_{sys_{cloudy}} = a_{sys_{cloudy}} - a_{ice_{cloudy}} \tag{2b}$$

Since the Arctic is frequently cloudy during the summer, we weighted the system albedo to appropriately incorporate clear and cloudy sky conditions. To do this, we assume that the sky is cloud-covered 80% of the time and clear the remaining 20% following the climatological cloud cover (Environmental Working Group, 2000). We then calculated a weighted average of the TOA albedo change (Δa_{Tm}) from bare ice to snow-covered ice under both sky conditions (Equation 3):

$$\Delta a_T = \left(0.2 \cdot \Delta a_{sys_{clear}}\right) + \left(0.8 \cdot \Delta a_{sys_{cloudy}}\right) \tag{3}$$

We used the results from the ice parcel database of the average areal coverage of events (IA_m) and the snow cover duration (D_m) to determine the change in the TOA radiative forcing (ΔRF) resulting from a TOA albedo change (Δa_T) of freshly accumulated snow on sea ice across the Arctic Ocean region:

$$\Delta RF_{Arctic\ Ocean} = \frac{1}{12}\sum_{m=1}^{12}\left(-\Delta a_T\right) \cdot F_m \cdot D_m \cdot \frac{IA_m}{A_{AO}} \tag{4}$$

where F_m is the TOA irradiance, A_{AO} is the Arctic Ocean domain, and monthly values are denoted by the subscript $_m$. The areal coverage of events (IA_m) needs to account for multiple snow accumulation events at a given parcel, the average sea ice coverage per month, and the average number of parcels that experience events per month. The term (IA_m) can be expanded into:

$$IA_m = \left(\frac{N_m}{C_m}\right) \cdot A_m \cdot SIC_m \tag{5}$$

Where the average number of events per month is (N_m); the average number of parcels per month is (C_m); the average number of parcels experiencing an event per month is (A_m) (multiplied by the grid cell area); and the corresponding average ice concentrations from ice parcels experiencing events per month is (SIC_m).

We combined Equations 4 and 5 into Equation 6 to compute the change in the TOA radiative forcing:

$$\Delta RF_{Arctic\ Ocean} = \frac{1}{12}\sum_{m=1}^{12}(-\Delta a_T)\cdot F_m \cdot D_m \cdot \left(\frac{N_m}{C_m}\right)\cdot\left(\frac{A_m \cdot SIC_m}{A_{AO}}\right) \quad (6)$$

Using Equation 6, we computed the monthly change in the TOA radiative forcing by multiplying the following variables: change in TOA albedo (Δa_{Tm}); the TOA irradiance (F_m); the average snow cover duration (D_m) as a fraction of the month (divided by 30.5); the average number of events per month (N_m); the average number of parcels per month (C_m); the average number of parcels experiencing an event per month (A_m) (multiplied by the grid cell area); and the corresponding average ice concentrations (SIC_m) from ice parcels experiencing events per month. We divided the result by the area of the Arctic Ocean (A_{AO}) to get the change in TOA radiative forcing over the Arctic Ocean domain. To get an annual average of the change in TOA radiative forcing ($\Delta RF_{Arctic\ Ocean}$), we summed the monthly radiative forcing across all months and divided by 12. The end-result is the change in the TOA radiative forcing that summer snow events have on a pan-Arctic scale averaged over 2003–2017.

4. Results

The approach for this study is broken down into three sections. First, Section 4.1 looks at the local scale using IMB buoy case examples of summer snow accumulation. This provides a source of direct measurements to compare against when looking at other environmental variables from the ice parcel database. Section 4.2 expands these events to the pan-Arctic scale using satellite, model, and reanalysis data from the Lagrangian ice parcel database to characterize summer snowfall patterns and the impacts of such events on surface albedo. Finally, Section 4.3 uses the areal coverage and duration results from Section 4.2, in situ albedo data, and the simple scattering model to quantify the potential TOA radiative forcing effects of summer snowfall on Arctic sea ice.

4.1. Local Scale Results

First, we present the details of one example case study from the 2008E buoy and its corresponding ice parcel as an example of the analysis applied to all case studies (Section 4.1.1). Following this are the collective results from all case studies and corresponding ice parcels at the local scale (Section 4.1.2).

4.1.1. Case Study: IMB 2008E

Here, we show a comparison between an IMB buoy and its corresponding ice parcel. It is important to remember that the IMB data only represents a single point in space, while the ice parcel covers a 25-km-by-25-km grid cell when interpreting the results. Between 8 July and 14 July 2008, 6 cm of snow accumulated at the 2008E buoy north of Greenland and persisted until 23 July. According to the buoy snow depths at the coincident ice parcel, the largest snowfall occurred on 12 July, which aligns with the SnowModel-LG simulated snow depth and ERA5 snowfall (Figure 1b). As the snow depth increased, there were distinct increases in the surface albedo and ice concentration of the ice parcel. A closer look into the observed meteorological conditions shows that buoy temperatures were below freezing (Figure 1e), there were high wind speeds (Figure 1f), and a decrease in sea level pressure (Figure 1g), all of which point to stormy weather.

In this case, the snow accumulation was the result of a nearby cyclone, as identified in the ice parcel database. Cyclones are often associated with high winds, which can compress the sea ice and close leads through convergence. Accordingly, an albedo increase during a snowfall event may not be solely due to fresh snow accumulation but could also result from the convergence of ice floes. Furthermore, freezing temperatures persisted throughout and after the snowfall event, which likely contributed to the decrease in satellite-derived melt pond coverage from 16.2% to 14.7% during the first 3 days of the event. Combined, these factors indicate a widespread coverage of new snow accumulation, which likely contributed to the positive shift in the reflectance distribution of the ice parcel domain (Figure S1 in Supporting Information S1).

4.1.2. Summary of Case Studies

The summary of all buoy data shows that the average observed snow accumulation occurred over 5.4 days, and the snow cover lasted for an average of 13.7 days after the first day of snowfall. The mean snow accumulation

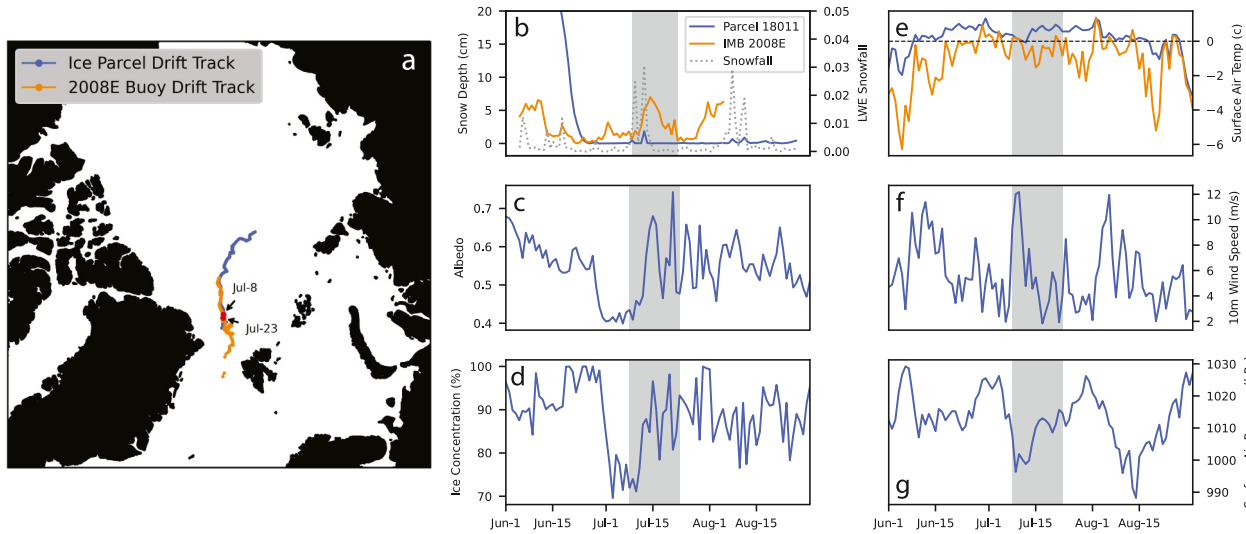

Figure 1. Time-series from IMB 2008E and its coincident ice parcel from June through August with the snow accumulation event (see Table S1 in Supporting Information S1) shaded in gray. Panels show (a) the drift track of IMB 2008E and Parcel 18011 from the ice parcel database, (b) snow depth measured by the IMB (orange), modeled snow depth from SnowModel-LG in the ice parcel database (blue), and ERA5 snowfall (dotted gray), (c) CERES albedo, (d) ice concentration from the NSIDC product, (e) surface air temperature from the IMB and ERA5 temperatures from the ice parcel database, (f) ERA5 10 m wind speeds, and (g) ERA5 surface air pressures. Note, the IMB time-series is from a point measurement, whereas the ice parcel time-series is from a 25-km-by-25-km grid cell.

amount was 6.5 cm (standard deviation: 3.5 cm). All buoy case studies were combined with corresponding ice parcels in space and time for an intercomparison of environmental conditions during snow accumulation events. Buoy data were then correlated with ice parcel variables using a Pearson correlation coefficient to assess the relationships between surface and atmospheric conditions during the snow accumulation events.

Figure 2 shows correlations between buoy and ice parcel variables from days during which the buoy snow depth increased. Interestingly, the buoy and SnowModelLG snow depths have a weak, negative correlation, and the relationship is not statistically significant. One possible reason for this may be the different spatial scales between the two data sets and the timing of snow accumulation. Cyclone systems tend to occur at the meso-scale, and the leading edges of the systems can arrive at a different time for a point measurement than for a 25 km^2 grid cell. When considering the relationship between the buoy and ice parcel variables throughout the duration of freshly accumulated snow, the correlations strengthen (Figure S2 in Supporting Information S1). However, the correlation between the simulated and observed snow depth remains negative and statistically insignificant. The lack of statistical significance between the modeled and IMB snow depths emphasizes the need for further evaluation of the simulated snow depths, which can be aided by in-depth comparisons as more buoys become available from ongoing and future deployments.

Other correlations reveal an insightful relationship between snowfall, surface albedo, and large-scale atmospheric conditions. Air temperatures are inversely correlated with albedo, snow depth, and ice concentration, which points to summer snow accumulation being a combined result of low pressure systems and cool temperatures at the surface and aloft. The correlation between simulated snow depth and the satellite-derived surface albedo is positive and statistically significant; however, the IMB snow depth data shows no statistically significant correlation with the surface albedo. This may be due to the smaller spatial footprint of the IMBs relative to an albedo retrieval over a native 20-km CERES resolution. Interestingly, ERA5 surface temperatures during snowfall periods decreased over the course of the summer. For correlations between variables during the entire snow cover duration, we refer readers to Figure S2 in Supporting Information S1.

4.2. Pan-Arctic Scale Results

Using the ice parcel database, we characterized the frequency, spatial extent, albedo change, and snow conditions associated with each snow accumulation event over the 2003–2017 period on the pan-Arctic scale. We define snow accumulation events using the same methodology as in the IMB local scale analysis. In general, snow accumulation events occur most frequently in the East Siberian, Chukchi, and Beaufort Seas with ~6 events per

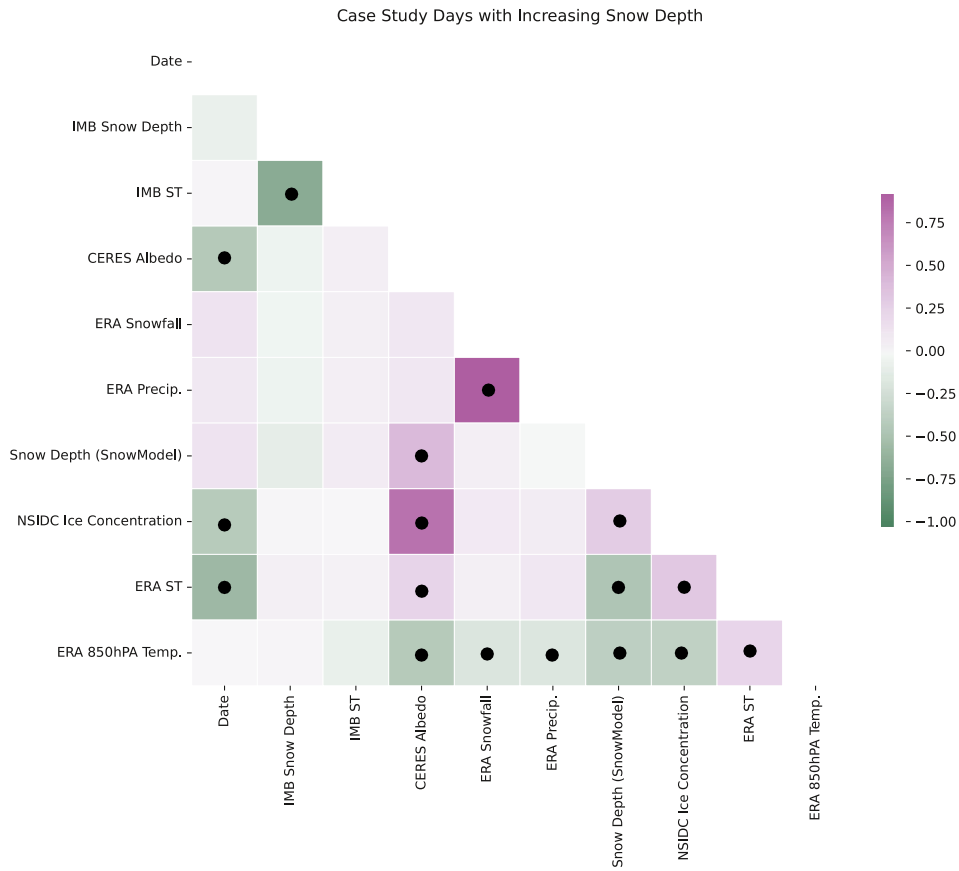

Figure 2. Pearson correlation values for case study IMBs and corresponding ice parcels using days when the snow depth increased at the buoys. Black dots represent 95% statistical significance. The results include cases where snow did not melt before the end of August. A corresponding figure based on the total duration of the freshly accumulated snow cover is shown Figure S2 in Supporting Information S1.

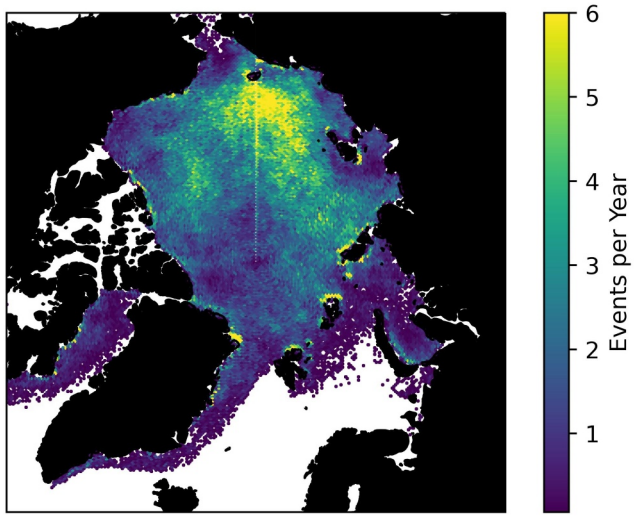

Figure 3. Density map showing where snow accumulation events occurred based on SnowModel-LG results from the ice parcel database in 2003–2017. Some locations experienced more than six events per year on average.

grid cell per year on average compared to one or fewer across most of the Greenland and Barents Seas (Figure 3). In the Pacific and Central Arctic regions, most events occur in July and early August, while the Atlantic regions (Barents, Greenland, Kara, Labrador, and Laptev) experience events at a consistent rate throughout the summer. The relative lack of events in the Atlantic region is likely a combined result of earlier seasonal ice loss (Cavalieri & Parkinson, 2012; Stroeve et al., 2014), generally higher temperatures and, as a consequence of higher temperatures, more rainfall rather and less snowfall (Boisvert et al., 2023). Note that, while snow could be falling at the same rate in all regions, the lower ice concentrations in one region would prevent high fractional coverage of fresh snow accumulation.

It is often assumed that snow can fall only when temperatures are below freezing, despite snow accumulation in above-freezing temperatures being possible. To quantify how often snow accumulation in above-freezing temperatures occurs, we examined the temperatures at two m ("surface") and at 850 hPa, as well as the albedo change, during the snow accumulation events. Figure 4 compares the distribution of temperatures at the surface and at the 850-hPa level and demonstrates that a high number of snowfall events in above-freezing temperatures occurs across the Arctic. On average, 60% of the snow accumulation events occurred in temperatures above 0°C at the 850-hPa level (Figure 4a). During these snow accumulation events, the surface albedo

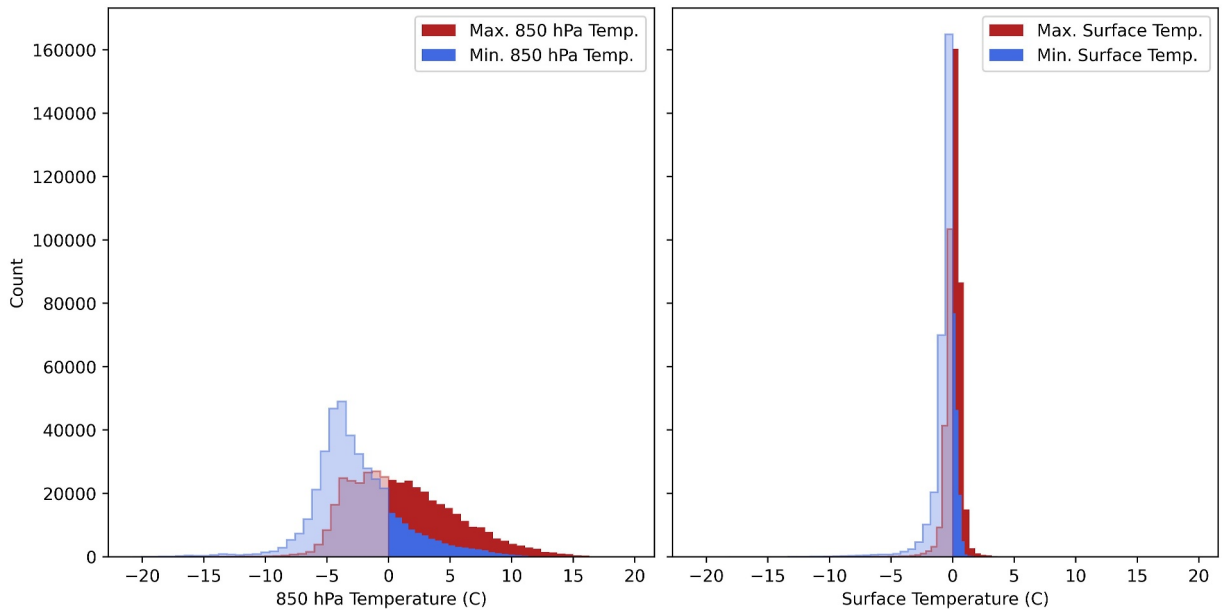

Figure 4. Temperature distributions across all snow accumulation events at the (a) 850-hPa level and (b) surface (2 m) level. Values come from the daily mean temperature from ERA5 in the ice parcel database. The figures show the maximum and minimum temperature during each event.

increased by 0.06. In comparison, when snow accumulated in above freezing 2-m temperatures (Figure 4b), the surface albedo increased 98% of the time, by an average value of 0.07. Through July and August, surface temperatures during events remained fairly similar to temperatures when no snowfall occurred, and rarely warmed above 0°C.

Next, we investigated the pan-Arctic changes in albedo resulting from snow accumulation events. Since even a very thin layer of snow can result in a fairly large albedo increase, we present the albedo minimum and maximum from the day with the thinnest and thickest snow layers alongside the minimum and maximum albedo during the event in Table 3. For 2003–2017, the average albedo at Day 0 of an event (bare ice conditions) was 0.47, and the average albedo on the day with the deepest snow during the event was 0.49, or an albedo increase of 0.02 (Table 3). When considering the lowest and highest albedo during the event, not tied to the thinnest or thickest snow depth, the average albedo changed from 0.44 to 0.52, yielding an albedo increase of 0.08. By comparing the maximum albedo change throughout the events with albedo change from the thinnest to thickest snow depths, we highlight that snow depth may not be a good predictor of albedo change. For instance, if the snow cover is already optically thick, an increase in snow depth will have little effect on the surface albedo.

When comparing the average event albedo by region (Figure 5a), geographic differences appear. The Greenland and Barents Seas show much lower albedos than any other region, while those in the Central Arctic are highest. Other regions have comparable albedos, being close to the 0.50 average for all snow accumulation events. Interestingly, the same regions with the lowest average albedo also experience the greatest increase in albedo from snow accumulation events (Figure 5b). Since relatively few events occur in the Greenland and Barents regions (Figure 3, Figure S3 in Supporting Information S1) despite lying within the North Atlantic storm track (Simmonds et al., 2008; Zhang et al., 2023), we speculate that their low average albedo is a result of low ice concentrations and generally high rates of surface melt associated with the lower latitude. More simply, even if many storm systems occur, there is less ice cover for the snow to accumulate on than in other regions. When conditions are favorable for accumulation, however, the fresh snow can lead to a larger temporary increase in albedo than that seen in regions with higher ice coverage.

To characterize the duration of events, we created two categories: thin snow accumulation events (maximum snow depth less than 3 cm) and thick snow accumulation events (maximum depth at least 3 cm). Overall, optically thick snow events lasted an average of 3.4 days longer than optically thin events (Table 3). This is likely a result of thicker snow taking more energy and, thus, time to melt completely, but it could also be related to other

Table 3
Average Albedo Values on the Day of the Event With Minimum and Maximum Snow Depth, Average Minimum and Maximum Albedo Throughout the Events, and the Duration of Events With a Thick (>3 cm) and Thin (<3 cm) Snow Accumulation

Year	Albedo: Day of min. snow	Albedo: Day of max. snow	Albedo min. throughout event	Albedo max. throughout event	Duration: Thick snow (>3 cm) [days]	Duration: Thin snow (<3 cm) [days]
2003	0.49	0.51	0.46	0.54	5.3	2.8
2004	0.50	0.52	0.47	0.55	5.4	2.6
2005	0.47	0.49	0.44	0.51	5.7	2.6
2006	0.49	0.51	0.47	0.53	6.5	2.7
2007	0.48	0.51	0.46	0.53	7.6	2.7
2008	0.48	0.49	0.45	0.52	5.9	3.0
2009	0.47	0.49	0.44	0.51	7.2	3.1
2010	0.45	0.46	0.42	0.49	6.0	2.7
2011	0.39	0.39	0.36	0.42	5.9	3.1
2012	0.45	0.46	0.41	0.49	6.5	3.1
2013	0.48	0.50	0.45	0.53	7.1	3.2
2014	0.48	0.49	0.45	0.52	7.2	2.7
2015	0.49	0.50	0.46	0.53	6.7	2.6
2016	0.49	0.51	0.46	0.53	5.3	2.8
2017	0.49	0.51	0.46	0.53	5.9	3.0
Average	0.47	0.49	0.44	0.52	6.3	2.8

atmospheric conditions associated with enhanced snowfall, such as lower temperatures (i.e., Lim et al., 2022) or increased cloudiness (Perovich, 2018).

In order to investigate the relationship between the event duration and other variables, we computed the correlations between duration and other potentially important factors. Of all variables, only snow depth showed a statistically significant (at least 95%) positive correlation, with an R^2 value of 0.58. This suggests that the main driver in the relationship between snow depth and duration is the time required to melt a deeper snow cover. Similar findings hold when the parcels are grouped by region and averaged over the entire period.

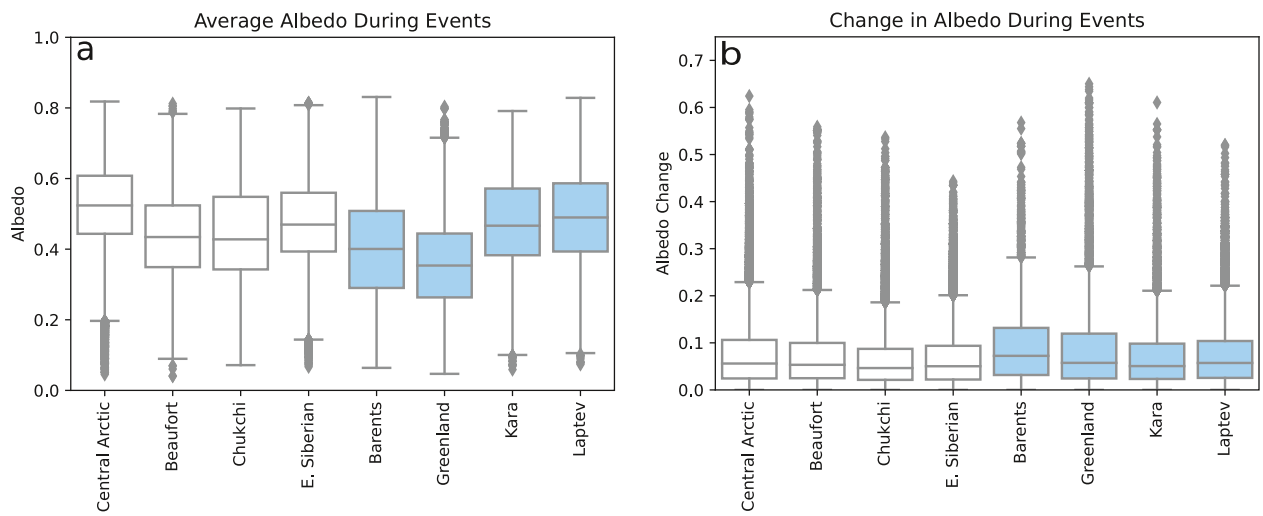

Figure 5. (a) The albedo for all snow accumulation events in each region over 2003–2017. (b) The average change in albedo during snow accumulation events in each region over 2003–2017. White boxes represent the central and Pacific Arctic sectors and blue represents the Atlantic and Eastern Arctic sectors. Diamonds show the outliers.

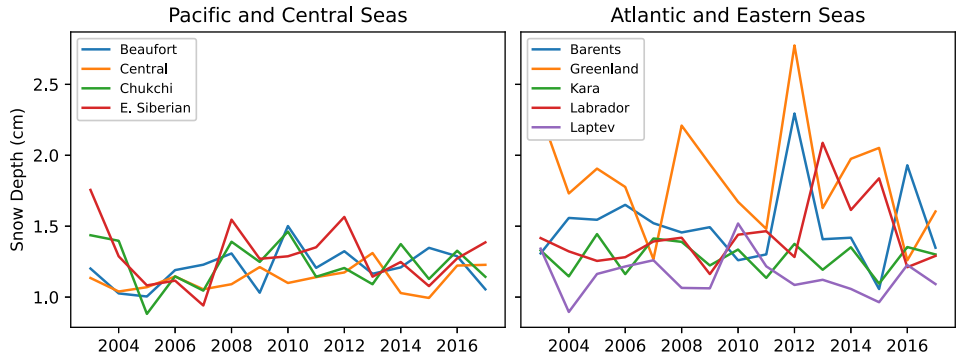

Figure 6. Regional average snow depth during snow accumulation events for 2003–2017.

Since snow depth plays an important role in the duration of the events, we looked further into the factors that may impact variations in snow depth. By comparing average event snow depth across regions, we expect to find deeper snow in the N. Atlantic sector since this area is known to have higher precipitation and snowfall rates than other regions of the Arctic. Figure 6 largely confirms this prediction. It is important to note that while the Atlantic and Eastern regions have a considerably deeper average snow depth, the Central and Pacific regions had far more events by region area (Figure S3 in Supporting Information S1). There are regional exceptions to this, such as the E. Laptev Sea; however, the Atlantic sector exhibits larger snow depth and interannual variability than the Pacific sector on average. It is likely that the storms in the Atlantic region, which are generally larger and contain more moisture than those in the Central Arctic and Pacific regions, are more likely to precipitate rain rather than snow. While N. Atlantic snow accumulation events are less frequent, the storm systems produce considerably more snow than those in other regions.

4.3. Radiative Forcing From Summer Snowfall

Here, we present the TOA radiative forcing change resulting from the accumulation of a fresh snow layer on top of bare sea ice using the two-layer albedo model of Thomas and Stamnes (1999, Section 6.11) in Equations 1a and 1b. We used surface albedo and transmittance values from optical measurements of thin (<3 cm) snow on ice (Brandt et al., 2005; Perovich, 2007). We determined the surface system albedo (a_{surf}) of a fresh snow cover over bare ice in clear skies and cloudy skies, yielding a combined system albedo (snow on top of ice) of 0.80 and 0.86, respectively (Equation 1). The TOA albedo for the combined system was 0.66 for clear skies $\left(a_{sys\,clear}\right)$ and 0.78 for cloudy skies $\left(a_{sys\,cloudy}\right)$ (Equation 2). Accounting for all sky conditions, we calculated a weighted average TOA albedo of 0.76 (a_T) (Equation 3). The change in TOA albedo (Δa_T) from bare sea ice to a thin layer of fresh snow is 0.12 (Equation 3).

From the pan-Arctic scale results in Section 4.2, we used the average spatial extent, frequency, and duration of snow accumulation events over the 15-year study period to determine the Arctic-wide radiative forcing effect. Table 4 shows the monthly values of each variable and the change in TOA radiative forcing resulting from new snow accumulation over bare sea ice. The uncertainties for variables are known estimated values (i.e., 15% ice concentration uncertainty), follow those in Webster and Warren (2022) (e.g., 0.0004% of the TOA solar irradiance), or are standard errors where applicable (e.g., for A_m, the number of ice parcels experiencing events).

Although peak insolation occurs in June, the greatest impact of summer snow accumulation events on TOA radiative forcing occurs in July, when the largest fraction of Arctic sea ice is snow-free and dominated by bare, melting ice. The dampening effect of the cloud cover at TOA throughout the summer is highlighted in Figure 7, which indicates that unusually cloudy conditions can lessen the radiative forcing by an average of 0.009 W m^{-2} throughout the summer, and by as much as 0.200 W m^{-2} in July.

Using Equation 6, we found the annual Arctic radiative forcing of summer snow accumulation to be -0.086 W $m^{-2} \pm 0.020$ W m^{-2}. Note that the similarity to the 0.08 albedo increase resulting from snow accumulation is coincidental. For context, if all Arctic sea ice were to melt during the sunlit season, there would be a TOA increase of 21 W m^{-2} of energy absorbed relative to 1979 ice coverage (Pistone et al., 2019). While our results show that summer snow events contribute only -0.086 W m^{-2} to the annual Arctic energy balance, every

Table 4
Average Monthly Values From Snow Accumulation Events in 2003–2017 Used in Equation 6 to Calculate the Change in the TOA Radiative Forcing Over the Arctic Ocean Domain

		May	June	July	August
Δa_T	Albedo Change at TOA from fresh snow			0.12	
				0.03	
F_m	TOA solar irradiance (W m^{-2})	412	498	460	314
		0.2	*0.2*	*0.2*	*0.1*
D_m	Average event duration (days)	8.0	2.7	2.8	4.1
		0.6	*0.1*	*0.1*	*0.2*
N_m	Arctic average event count	1554	6,375	12,644	8,062
		40	*243*	*325*	*217*
C_m	Average number of parcels	20,247	17,509	13,155	9,020
		40	*40*	*58*	*63*
A_m	Average number of parcels that experienced events	732	2619	3,976	3,206
		15	*72*	*71*	*65*
SIC_m	Average sea ice concentration	69.6%	78.5%	72.3%	72.2%
		15%	*15%*	*15%*	*15%*
IA_m	Area of summer snow accumulation (km^2)	24,439	467,847	1,726,865	1,293,055
A_O	Area of the Arctic Ocean (km^2)			17.1×10^6	
$(A_m * SIC_m * 25\text{ km} * 25\text{ km})/A_{AO}$	Fraction of Arctic ocean changed from ice to fresh snow	1.9%	7.5%	10.5%	8.5%
$RF_{Arctic\ Ocean}$	Change in TOA radiative forcing (W m^{-2})	−0.018	−0.143	−0.495	−0.370
		−0.004	*−0.031*	*−0.114*	*−0.086*

Note. Uncertainties for each result are presented in italics.

small amount of cooling is important when considering the large ecological and socioeconomic changes that are a consequence of Arctic sea ice loss.

5. Discussion

The results presented here reveal the frequency, duration, and magnitude of summer snow accumulation events and the role they play in the Arctic energy balance. However, these analyses assume surfaces are completely covered by fresh snow and that sea ice concentration is invariable. In reality, a situation in which there is no change in surface conditions or ice concentration during snow accumulation events is highly unlikely. In Section 5.1, we investigate the impact of ice concentration and melt pond coverage on surface albedo. Section 5.2 compares this work with other studies of Arctic summer snowfall.

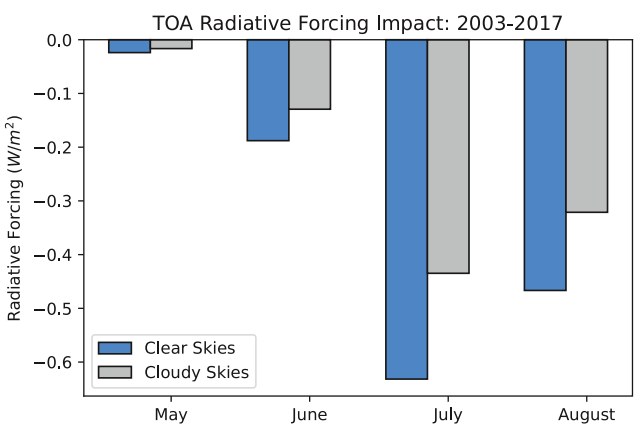

Figure 7. The change in TOA radiative forcing in clear and cloudy sky conditions from snow accumulation events over the Arctic Ocean in 2003–2017.

5.1. Alternative Sources of Albedo Change

We found evidence that ice concentration could play a role in the albedo changes during snow accumulation events from the case studies and ice parcel database results. We further investigated the ice concentration change and melt pond coverage during snow accumulation events in order to distinguish the different sources of albedo change.

To estimate the effects of sea ice convergence on albedo, we performed a back-of-the-envelope calculation of the evolution of the aggregate-scale albedo during snow accumulation events following Perovich, Light, et al. (2007). The aggregate-scale albedo is an estimate of the surface albedo based on the fractional coverage of different surface types within a 25-km-by-25-km area and their known broadband albedos. The calculation assumes

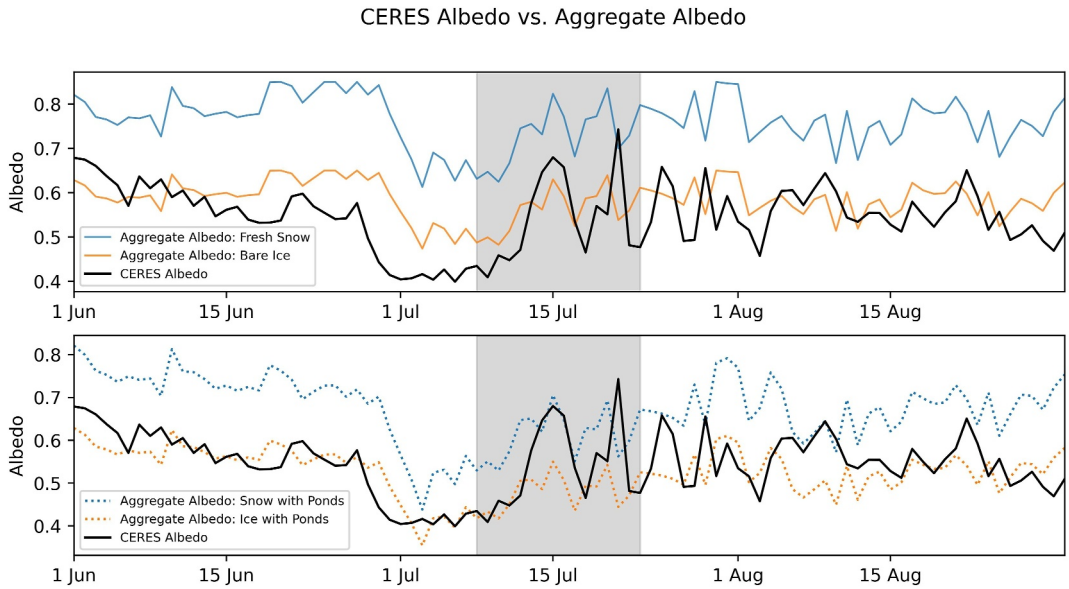

Figure 8. CERES albedo from the ice parcel database for the 2008E event (dates shaded in gray) compared with computed aggregated albedos using (a) fresh snow and bare ice albedos and sea ice concentration and (b) snow, bare ice, and melt pond albedos, melt pond fraction, and sea ice concentration.

linear scaling in albedos of surface types and does not capture the meter-scale heterogeneity or the subtle physical transitions between surface types at the meter-scale; however, the method is an effective means for evaluating the aggregate-scale albedo transition from snow-free to snow-covered sea ice.

We used in situ albedos of four different surface conditions (bare sea ice, fresh snow, bare ice with melt ponds, and snow-covered ice with melt ponds), and satellite retrievals of sea ice concentration and melt pond fraction. We began with ice concentration values from the ice parcels coincident with IMB buoys assuming bare sea ice and open water were present (Equation 7a):

$$a = (a_{ice} * SIC) + (a_o * (1 - SIC)) \tag{7a}$$

where a represents the aggregate albedo of a given ice parcel, a_{ice} is the bare sea ice albedo (0.65) (Light et al., 2022; Perovich et al., 2002), a_o is the open water albedo (0.07) (Pegau & Paulson, 2001), and SIC is the ice parcel ice concentration. By replacing the bare sea ice albedo (a_{ice}, 0.65) with that of fresh snow (0.85) (Light et al., 2022; Perovich et al., 2002) in Equation 5a, we compared the aggregate albedos of the two scenarios (bare ice with open water and snow-covered ice with open water) with the satellite-derived albedo of the ice parcel for the 2008E case study. In this case, we found that the expected albedo for bare ice was higher than the ice parcel albedo, implying that the ice surface had developed melt ponds.

To investigate this further, we modified Equation 7a to include three surface types: bare sea ice, melt ponds, and open water, as shown in Equation 7b:

$$a = a_{ice} * (SIC - MPF) + (a_{mp} * MPF) + (a_o * (1 - SIC)) \tag{7b}$$

where a_{mp} represents the albedo of melt ponds (0.22) (Light et al., 2022; Perovich et al., 2002), and MPF is the melt pond fraction of the ice area, integrated to daily values based on the 8-day composite product from Rösel et al. (2015). We replace the bare ice albedo variable (a_{ice}, 0.65) with that of fresh snow (0.85) in Equation 7b to evaluate the differences in aggregate albedo between bare ice with melt ponds and snow-covered ice with melt ponds.

From these results, we conclude that during the 2008E case study, the surface was mostly bare, melting sea ice with melt ponds prior to the accumulation event (Figure 8). During the snow accumulation event (July 8–14), the

satellite-derived albedo (black line) increased to that of fresh snow with melt ponds (~July 15) (dashed blue line) before decreasing to bare sea ice (~July 18) (dashed orange line). While the satellite-derived albedo did not remain high after the snow melted, the albedo remained distinctly higher than the period before the snowfall, which is likely due to the partial refreezing of melt ponds. As observed during ephemeral freezing and snowfall (e.g., Webster et al., 2022), larger melt ponds can remain "open" in windy conditions and near-zero temperatures, while smaller ponds can develop ice lids and accumulate snowfall. The meteorological conditions at IMB 2008E reveal that the snowfall event began in windy, near-zero surface temperatures (Figure 1, panels e–f), which would have inhibited the freezing of larger melt ponds, preventing snow accumulation over the entire ice surface. Since our back-of-the-envelope estimate accounts for changes in sea ice concentration, the albedo increase during the snowfall event can be primarily attributed to a change in the surface albedo of the ice cover rather than to ice convergence.

Applying the same calculation to all IMB case studies, we found that the average ice parcel albedo was most similar to that of bare ice with ponds initially, and ranged closer to snow-covered ice with melt ponds during the event (Figure S4 in Supporting Information S1). Our results suggest that some ponds remained unfrozen during the snow accumulation events, which has been observed in situ before (e.g., Webster et al., 2022). Alternatively, the albedo could have increased instead from fresh snow covering a fraction of the ice surface through wind-driven snow redistribution.

In Section 4.3, we calculated radiative forcing of snow accumulation by assuming that all ice surfaces were completely covered by fresh snow and no melt ponds were present. We found that the satellite-derived (CERES) albedos during snow accumulation events are most similar to snow-covered ice with melt ponds than to a fully snow-covered ice surface. This suggests that the radiative forcing estimates are likely an overestimate; however, more detailed analysis incorporating melt pond coverage is needed to constrain the potential bias. It is important to note that the products used here also include their own inherent biases. For example, the CERES albedo product tends to overestimate downwelling shortwave radiation and underestimate upwelling shortwave (Huang et al., 2022), which leads to an underestimate in the surface albedos used in this analysis.

5.2. Comparative Work

This work complements the results presented by Lim et al. (2022), specifically those related to albedo, despite the different criteria used to define summer snowfall events. The Lim et al. (2022) analysis defines a snowstorm as occurring "when the daily snowfall averaged over the Eurasian-Pacific sector of the Arctic (80–240°E; 69–90°N) exceeds 0.75 standard deviations for 3 or more consecutive days"; however, the results of both methods are complementary. For example, they estimated that a 0.01 increase in albedo may increase upwelling shortwave radiation at the surface by 2.0–3.5 W m^{-2} based on the CERES climatological mean (2000–2019). Our results from Equation 6 for June–August 2003–2017 (excluding May for an equivalent comparison) show a change of -12.3 W m^{-2} at the surface when considering an 80% cloud cover and a 203 W m^{-2} mean surface irradiance (Hartmann, 2016) as done by Lim et al. (2022). While including cloud cover in our estimate decreases the amount of energy reflected at the surface, the main difference between our findings is based on the different definitions of a snow event. Namely, since our events start with no snow on the ice surface, the increase in surface albedo during the event will generally be greater than if a snow layer was already present. Despite the different methodologies, we also found an average of ~2 snow accumulation events per grid cell in the Arctic each year, which agrees with the Lim et al. (2022) study's 2–3 storm events per year.

6. Conclusion

Until recently, there have been gaps in the scientific literature regarding summer snow on Arctic sea ice. Investigations of individual snowfall events reveal the importance of summer snow accumulation in the local energy balance (Perovich et al., 2017), and the role of storm systems on surface albedo during summer (Lim et al., 2022). However, little has been done to expand local-scale surface processes to the broader Arctic on these topics. By analyzing observations, satellite, and reanalysis data across the Arctic, this study bridges the gap by quantifying the frequency and extent of summer snow accumulation on sea ice and calculating the snow layer's role in reflecting incoming shortwave radiation from the Arctic sea-ice surface using observationally based methods.

We found that, across the Arctic, ∼2 snow accumulation events occurred per grid cell on initially snow-free conditions each year. The average snow depth and albedo increases were ∼2 cm and 0.08, respectively. 16.5% of the snow accumulation events were optically thick (>3 cm deep) and lasted 2.9 days longer than the average snow accumulation event (3.4 days). Based on a simple, multiple scattering radiative transfer model, we estimated a -0.086 ± 0.020 W m^{-2} change in the annual average radiative forcing for summer snowfall events in 2003–2017. These results can provide a valuable basis for climate models to be assessed by (e.g., Light et al., 2015), as they represent a more complete picture of summer snowfall and the Arctic energy balance over sea ice.

There are several other ways in which snow can impact the sea ice environment in summer beyond the results shown here. When sea ice is actively melting, fresh snow accumulation can cool the ice surface as a result of latent heat loss from the ice as the snow melts. The magnitude of this effect varies with snow density and temperature, but it can be enough to postpone the onset of surface melt and the formation of melt ponds (Perovich et al., 2017).

The greatest radiative forcing impact from snow accumulation occurs in July with the combination of high downwelling shortwave radiation and melt conditions persisting across the Arctic, but more work is needed to investigate the complex processes occurring in the early spring and autumn. Although not included in this study, it is common for snow to accumulate on top of an existing snowpack during these periods. If the existing snowpack is old or melting, it will have a slightly lower albedo than that of fresh snow and would therefore would also be expected to have a negative radiative forcing effect (Perovich & Polashenski, 2012). As the Arctic climate continues to warm, with melt onset beginning earlier and freeze-up occurring later in the year (Bliss et al., 2019; Stroeve et al., 2014), the effects of snow accumulation during the shoulder seasons will likely play an increasingly important role in the seasonal evolution of Arctic sea ice mass balance.

Data Availability Statement

IMB buoy data is produced by the CRREL Mass Balance Buoy Program (Perovich et al., 2023). The Ice Parcel Database (Horvath et al., 2023) is available on Zenodo at: https://zenodo.org/records/6646932. Melt pond fractions (Rösel et al., 2015) are available from the World Data Center for Climate at DKRZ (doi:10.1594/WDCC/MODIS__Arctic__MPF_V02). Figures were made with Matplotlib (Hunter, 2007) version 3.8.2 (doi:10.5281/zenodo.592536). Maps were produced with SciTools Cartopy (Elson et al., 2023). Analysis for this manuscript was completed using Python version 3.9.7.

Acknowledgments
HRC conducted this work under NASA's Interdisciplinary Research in Earth Science program, project 80NSSC21K0264. MAW acknowledges support from the National Science Foundation Project: 2325430 and NASA Projects 80NSSC21K0264 and 80NSSC24K0901. We are grateful to Stephen Warren for constructive discussions regarding the radiative balance analysis. We thank Thomas Ballinger, Matthew Sturm, Simon Zwieback, and Emily Fedders for their helpful feedback. We also thank Ruzica Dadic, two anonymous reviewers, and editor Ping Yang for their constructive reviews.

References

Bliss, A. C., Steele, M., Peng, G., Meier, W. N., & Dickinson, S. (2019). Regional variability of Arctic sea ice seasonal change climate indicators from a passive microwave climate data record. *Environmental Research Letters*, *14*(4), 045003. https://doi.org/10.1088/1748-9326/aafb84

Boisvert, L. N., Webster, M. A., Parker, C. L., & Forbes, R. M. (2023). Rainy days in the Arctic. *Journal of Climate*, *36*(19), 1–48. https://doi.org/10.1175/JCLI-D-22-0428.1

Brandt, R. E., Warren, S. G., Worby, A. P., & Grenfell, T. C. (2005). Surface Albedo of the Antarctic Sea Ice zone. *Journal of Climate*, *18*(17), 3606–3622. https://doi.org/10.1175/jcli3489.1

Cabaj, A., Kushner, P. J., Fletcher, C. G., Howell, S., & Petty, A. A. (2020). Constraining reanalysis snowfall over the Arctic Ocean using CloudSat observations. *Geophysical Research Letters*, *47*(4), e2019GL086426. https://doi.org/10.1029/2019GL086426

Cavalieri, D. J., & Parkinson, C. L. (2012). Arctic sea ice variability and trends, 1979–2010. *The Cryosphere*, *6*(4), 881–889. https://doi.org/10.5194/tc-6-881-2012

Edel, L., Claud, C., Genthon, C., Palerme, C., Wood, N., L'Ecuyer, T., & Bromwich, D. (2020). Arctic snowfall from CloudSat observations and reanalyses. *Journal of Climate*, *33*(6), 2093–2109. https://doi.org/10.1175/JCLI-D-19-0105.1

Elson, P., Sales de Andrade, E., Lucas, G., May, R., Hattersley, R., Campbell, E., et al. (2023). SciTools/cartopy: v0.22.0 (v0.22.0). *Zenodo*. https://doi.org/10.5281/zenodo.8216315

Environmental Working Group. (2000). In F. Fetterer, & V. F. Radionov (Eds.). *Environmental working Group Arctic Meteorology and climate Atlas* Version 1 [Dataset]. National Snow and Ice Data Center. https://doi.org/10.7265/N5MS3QNJ

Fetterer, F., Knowles, K., Meier, W. N., Savoie, M., & Windnagel, A. K. (2017). *Sea ice index, version 3*. National Snow and Ice Data Center. https://doi.org/10.7265/N5K072F8

Fetterer, F., & Untersteiner, N. (1998). Observations of melt ponds on Arctic sea ice. *Journal of Geophysical Research*, *103*(C11), 24821–24835. https://doi.org/10.1029/98jc02034

Hartmann, D. L. (2016). *Global physical climatology*. Academic Press.

Hersbach, H., Bell, B., Berrisford, P., Biavati, G., Horányi, A., Muñoz Sabater, J., et al. (2023). ERA5 hourly data on single levels from 1979 to present. *Copernicus Climate Change Service (C3S) Climate Data Store (CDS)*. https://doi.org/10.24381/cds.adbb2d47

Horvath, S., Boisvert, L., Parker, C., Webster, M., Taylor, P., Boeke, R., et al. (2023). Database of daily Lagrangian Arctic sea ice parcel drift tracks with coincident ice and atmospheric conditions. *Scientific Data*, *10*(1), 73. https://doi.org/10.1038/s41597-023-01987-6

Huang, Y., Taylor, P., Rose, F., Rutan, D., Shupe, M., Webster, M., & Smith, M. (2022). Toward a more realistic representation of surface albedo in NASA CERES-derived surface radiative fluxes: A comparison with the MOSAiC field campaign: Comparison of CERES and MOSAiC surface radiation fluxes. *Elementa: Science of the Anthropocene*, *10*(1), 00013. https://doi.org/10.1525/elementa.2022.00013

Hunter, J. (2007). Matplotlib: A 2D Graphics environment. *Computing in Science and Engineering*, *9*(3), 90–95. https://doi.org/10.1109/MCSE.2007.55

Light, B., Dickinson, S., Perovich, D. K., & Holland, M. M. (2015). Evolution of summer Arctic sea ice albedo in CCSM4 simulations: Episodic summer snowfall and frozen summers. *Journal of Geophysical Research: Oceans*, *120*(1), 284–303. https://doi.org/10.1002/2014JC010149

Light, B., Smith, M. M., Perovich, D. K., Webster, M. A., Holland, M. M., Linhardt, F., et al. (2022). Arctic sea ice albedo: Spectral composition, spatial heterogeneity, and temporal evolution observed during the MOSAiC drift. *Elementa: Science of the Anthropocene*, *10*(1), 000103. https://doi.org/10.1525/elementa.2021.000103

Lim, W. I., Park, H. S., Petty, A. A., & Seo, K. H. (2022). The role of summer snowstorms on seasonal Arctic Sea Ice loss. *Journal of Geophysical Research: Oceans*, *127*(12), e2021JC018066. https://doi.org/10.1029/2021JC018066

Liston, G. E., Itkin, P., Stroeve, J., Tschudi, M., Stewart, J. S., Pedersen, S. H., et al. (2020). A Lagrangian snow-evolution system for sea-ice applications (SnowModel-LG): Part I – Model description. *Journal of Geophysical Research: Oceans*, *125*(10), e2019JC015913. https://doi.org/10.1029/2019jc015913

Meier, W., Stroeve, J., & Fetterer, F. (2007). Whither Arctic sea ice? A clear signal of decline regionally, seasonally and extending beyond the satellite record. *Annals of Glaciology*, *46*, 428–434. https://doi.org/10.3189/172756407782871170

Pegau, W. S., & Paulson, C. A. (2001). The albedo of Arctic leads in summer. *Annals of Glaciology*, *33*, 221–224. https://doi.org/10.3189/172756401781818833

Perovich, D., Polashenski, C., Arntsen, A., & Stwertka, C. (2017). Anatomy of a late spring snowfall on sea ice. *Geophysical Research Letters*, *44*(6), 2802–2809. https://doi.org/10.1002/2016GL071470

Perovich, D., Richter-Menge, J., & Polashenski, C. (2023). Observing and understanding climate change: Monitoring the mass balance, motion, and thickness of Arctic sea ice. http://imb-crrel-dartmouth.org

Perovich, D. K. (2007). Light reflection and transmission by a temperate snow cover. *Journal of Glaciology*, *53*(181), 201–210. https://doi.org/10.3189/172756507782202919

Perovich, D. K. (2018). Sunlight, clouds, sea ice, albedo, and the radiative budget: The umbrella versus the blanket. *The Cryosphere*, *12*(6), 2159–2165. https://doi.org/10.5194/tc-12-2159-2018

Perovich, D. K., Grenfell, T. C., Light, B., & Hobbs, P. V. (2002). Seasonal evolution of the albedo of multiyear Arctic sea ice. *Journal of Geophysical Research*, *107*(C10), 8044. https://doi.org/10.1029/2000JC000438

Perovich, D. K., Light, B., Eicken, H., Jones, K. F., Runciman, K., & Nghiem, S. V. (2007a). Increasing solar heating of the Arctic Ocean and adjacent seas, 1979–2005: Attribution and role in the ice-albedo feedback. *Geophysical Research Letters*, *34*(19), L19505. https://doi.org/10.1029/2007GL031480

Perovich, D. K., Nghiem, S. V., Markus, T., & Schweiger, A. (2007b). Seasonal evolution and interannual variability of the local solar energy absorbed by the Arctic sea ice–ocean system. *Journal of Geophysical Research*, *112*(C3). https://doi.org/10.1029/2006JC003558

Perovich, D. K., & Polashenski, C. (2012). Albedo evolution of seasonal Arctic sea ice. *Geophysical Research Letters*, *39*(8), L08501. https://doi.org/10.1029/2012GL051432

Pistone, K., Eisenman, I., & Ramanathan, V. (2019). Radiative heating of an ice-free arctic ocean. *Geophysical Research Letters*, *46*(13), 7474–7480. https://doi.org/10.1029/2019GL082914

Polashenski, C., Perovich, D., & Courville, Z. (2012). The mechanisms of sea ice melt pond formation and evolution. *Journal of Geophysical Research*, *117*(C1), C01001. https://doi.org/10.1029/2011JC007231

Post, E., Bhatt, U., Bitz, C., Brodie, J., Fulton, T., Hebblewhite, M., et al. (2013). Ecological consequences of sea-ice decline. *Science*, *341*(6145), 519–524. https://doi.org/10.1126/science.1235225

Rösel, A., Kaleschke, L., & Kern, S. (2015). Gridded melt pond cover fraction on Arctic Sea Ice derived from TERRA-MODIS 8-day composite reflectance data bias corrected version 02, https://doi.org/10.1594/WDCC/MODIS__Arctic__MPF_V02

Scharien, R. K., & Yackel, J. J. (2005). Analysis of surface roughness and morphology of first-year sea ice melt ponds: Implications for microwave scattering. *IEEE Transactions on Geoscience and Remote Sensing*, *43*(12), 2927–2939. https://doi.org/10.1109/TGRS.2005.857896

Simmonds, I., Burke, C., & Keay, K. (2008). Arctic climate change as manifest in cyclone behavior. *Journal of Climate*, *21*(22), 5777–5796. https://doi.org/10.1175/2008JCLI2366.1

Stroeve, J. C., Markus, T., Boisvert, L., Miller, J., & Barrett, A. (2014). Changes in Arctic melt season and implications for sea ice loss. *Geophysical Research Letters*, *41*(4), 1216–1225. https://doi.org/10.1002/2013GL058951

Sumata, H., Lavergne, T., Girard-Ardhuin, F., Kimura, N., Tschudi, M. A., Kauker, F., et al. (2014). An intercomparison of Arctic ice drift products to deduce uncertainty estimates. *Journal of Geophysical Research: Oceans*, *119*(8), 4887–4921. https://doi.org/10.1002/2013JC009724

Thomas, G. E., & Stamnes, K. (1999). *Radiative transfer in the atmosphere and ocean* (p. 517). Cambridge University Press.

Wang, C., Graham, R. M., Wang, K., Gerland, S., & Granskog, M. A. (2019). Comparison of ERA5 and ERA-Interim near-surface air temperature, snowfall and precipitation over Arctic sea ice: Effects on sea ice thermodynamics and evolution. *The Cryosphere*, *13*(6), 1661–1679. https://doi.org/10.5194/tc-13-1661-2019

Warren, S. G. (2019). Optical properties of ice and snow. *Philosophical Transactions of the Royal Society A*, *377*(2146), 20180161. https://doi.org/10.1098/rsta.2018.0161

Webster, M., Holland, M., Wright, N. C., Hendricks, S., Hutter, N., Itkin, P., et al. (2022). Spatiotemporal evolution of melt ponds on Arctic sea ice: MOSAiC observations and model results. *Elementa: Science of the Anthropocene*, *10*(1). https://doi.org/10.1525/elementa.2021.000072

Webster, M., Rigor, I. G., Perovich, D. K., Richter-Menge, J. A., Polashenski, C. M., & Light, B. (2015). Seasonal evolution of melt ponds on Arctic sea ice. *Journal of Geophysical Research: Oceans*, *120*(9), 5968–5982. https://doi.org/10.1029/2015JC011030

Webster, M. A., & Warren, S. G. (2022). Regional geoengineering using tiny glass bubbles would accelerate the loss of Arctic sea ice. *Earth's Future*, *10*, e2022EF002815. https://doi.org/10.1029/2022ef002815

Wielicki, B. A., Barkstrom, B. R., Harrison, E. F., Lee III., R. B., Smith, G. L., & Cooper, J. E. (1996). Clouds and the earth's radiant energy system (CERES): An earth observing system experiment. *Bulletin America Meteorology Social*, *77*(5), 853–868. https://doi.org/10.1175/1520-0477(1996)077<0853:catere>2.0.co;2

Zhang, X., Tang, H., Zhang, J., Walsh, J. E., Roesler, E. L., Hillman, B., et al. (2023). Arctic cyclones have become more intense and longer-lived over the past seven decades. *Communications Earth & Environment*, *4*(1), 348. Article 1. https://doi.org/10.1038/s43247-023-01003-0

References From the Supporting Information

Charlson, R. J., Langner, J., Rodhe, H., Leovy, C. B., & Warren, S. G. (1991). Perturbation of the northern hemisphere radiative balance by backscattering from anthropogenic sulfate aerosols. *Tellus*, *43*(4), 152–162. https://doi.org/10.1034/j.1600-0889.1991.t01-1-00013.x

Herman, G. F. (1977). Solar radiation in summertime Arctic stratus clouds. *Journal of the Atmospheric Sciences*, *34*(9), 1423–1432. https://doi.org/10.1175/1520-0469(1977)034<1423:srisas>2.0.co;2

Herman, G. F., & Curry, J. A. (1984). Observational and theoretical studies of solar radiation in Arctic stratus clouds. *Journal of Climate and Applied Meteorology*, *23*(1), 5–24. https://doi.org/10.1175/1520-0450(1984)023<0005:oatsos>2.0.co;2

Paltridge, G. W., & Platt, C. M. R. (1976). *Radiative processes in meteorology and climatology* (p. 318). Elsevier.

Wiscombe, W. J. (1975). Solar radiation calculations for Arctic summer stratus conditions. In G. Weller & S. A. Bowling (Eds.), *Climate of the Arctic* (pp. 245–254). University of Alaska Press.